

Distinct High Energy Cutoff Variation Patterns in Two Seyfert Galaxies

Jia-Lai Kang,^{1,2*} Jun-Xian Wang,^{1,2†} Wen-Yong Kang^{1,2}

¹CAS Key Laboratory for Research in Galaxies and Cosmology, Department of Astronomy, University of Science and Technology of China, Hefei, Anhui 230026, China

²School of Astronomy and Space Science, University of Science and Technology of China, Hefei 230026, China

Accepted 2021 January 4. Received 2020 December 22; in original form 2020 September 29

ABSTRACT

Investigating how the cutoff energy E_{cut} varies with X-ray flux and photon index Γ in individual AGNs opens a new window to probe the yet unclear coronal physics. So far E_{cut} variations have only been detected in several AGNs but different patterns have been reported. Here we report new detections of E_{cut} variations in two Seyfert galaxies with multiple NuSTAR exposures. While in NGC 3227 E_{cut} monotonically increases with Γ , the $E_{\text{cut}}-\Gamma$ relation exhibits a Λ shape in SWIFT J2127.4+5654 (E_{cut} increasing with Γ at $\Gamma \lesssim 2.05$, but reversely decreasing at $\Gamma \gtrsim 2.05$), indicating more than a single underlying mechanism is involved. Meanwhile both galaxies show softer spectra while they brighten in X-ray, a common phenomenon in Seyfert galaxies. Plotting all 7 AGNs with E_{cut} variations ever reported with NuSTAR observations in the $E_{\text{cut}}-\Gamma$ diagram, we find they could be unified with the Λ pattern. Although the sample is small and SWIFT J2127.4+5654 is the only source with Γ varying across the break point thus the only one exhibiting the complete Λ pattern in a single source, the discoveries shed new light on the coronal physics in AGNs. Possible underlying physical mechanisms are discussed.

Key words: Galaxies: active – Galaxies: nuclei – X-rays: galaxies

1 INTRODUCTION

In the standard disc-corona paradigm the hard X-ray emission of active galactic nuclei (AGNs) is produced in a hot and compact region, the so called corona (e.g. Haardt & Maraschi 1991; Haardt et al. 1994), through the inverse Compton scattering of the seed photons from the accretion disk. This process could produce the observed power law continuum with a high-energy cutoff. Such a cutoff has been detected in a number of AGNs (Zdziarski et al. 2000; Molina et al. 2013), particularly with the high-quality hard X-ray spectra of NuSTAR (e.g., Matt et al. 2015; Tortosa et al. 2018; Molina et al. 2019; Kang et al. 2020), providing key constraints on the yet unclear coronal physics (e.g. Fabian et al. 2015).

The Nuclear Spectroscopic Telescope Array (NuSTAR Harrison et al. 2013) also enables the detection of E_{cut} (or coronal temperature T_e) variations in individual AGNs with multiple exposures, including 3C 382 (Ballantyne et al. 2014), NGC 5548 (Ursini et al. 2015), Mrk 335 (Keek & Ballantyne 2016), NGC 4593 (Ursini et al. 2016; Middei et al. 2019a), MCG-5-23-16 (Zoghbi et al. 2017), and 4C 74.26 (Zhang et al. 2018). Zhang et al. (2018) also revisited the first five sources mentioned above using the spectra ratio technique they developed. They confirmed the claimed E_{cut} variations in 3 of them, but disproved those in NGC 4593 and MCG-5-23-16. Despite the limited number of sources, these studies have opened a new window to probe the coronal physics. Remarkably, Zhang et al. (2018) found that all the 4 AGNs with E_{cut} variations confirmed tend to have larger E_{cut} (thus hotter corona) when they brighten and soften in X-ray. In other words, they show a “hotter-when-brighter” behav-

ior along with the conventional “softer-when-brighter” pattern (e.g., Markowitz et al. 2003; Sobolewska & Papadakis 2009). Possible underlying mechanisms have been discussed in Zhang et al. (2018) and Wu et al. (2020), including geometrical changes of the corona and pair production. Do Seyfert galaxies universally follow this “hotter-when-softer/brighter” pattern? A possible counter-example is the narrow line Seyfert 1 galaxy (NLS1) Ark 564, for which Barua et al. (2020) found cooler corona (though statistically marginal) during the softer and brighter phases within a 200 ks NuSTAR observation.

In this letter we report new detections of E_{cut} variations in two Seyfert galaxies, NGC 3227 and SWIFT J2127.4+5654, and a Λ shaped $E_{\text{cut}}-\Gamma$ relation for the first time. §2 presents the NuSTAR observations and data reduction. In §3 we describe the spectral models and deliver the fitting results. In §4 we discuss the spectral variabilities and the underlying mechanisms for AGNs with reported E_{cut} variations.

2 OBSERVATIONS AND DATA REDUCTION

NGC 3227 is a radio-quiet Seyfert 1.5 galaxy (Véron-Cetty & Véron 2006) at $z = 0.0039^1$. In Tab. 1 we list the seven archival NuSTAR observations of NGC 3227. NGC 3227 shows highly variable X-ray emission and its absorption feature have been extensively investigated in literature. As an example, based on the NuSTAR and XMM-Newton observations, Turner et al. (2018) found a rapid occultation event in NGC 3227 between two exposures of NuSTAR (60202002010 and 60202002012), with several absorber zones in-

* ericofk@mail.ustc.edu.cn

† jxw@ustc.edu.cn

¹ The radio types and the redshifts are from NED: <http://ned.ipac.caltech.edu>

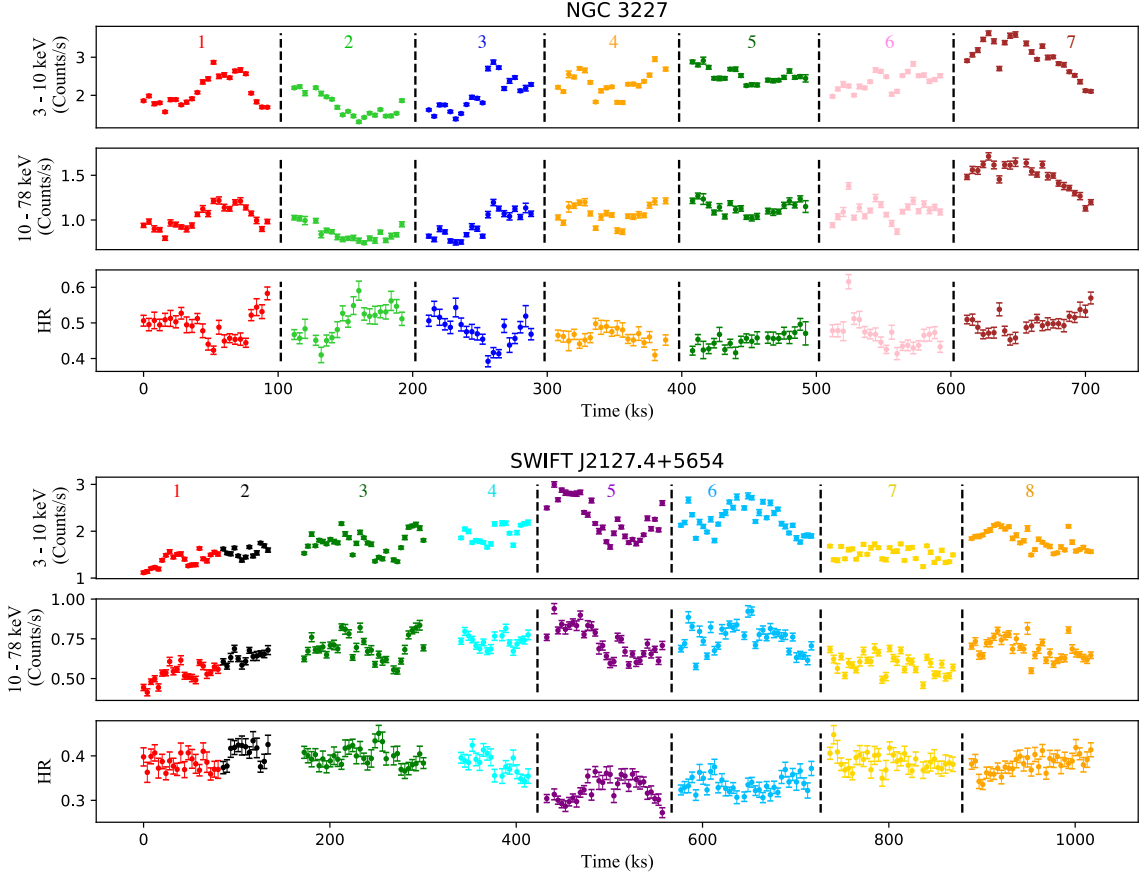


Figure 1. NuSTAR light curves (with a bin size of 4 ks) in 3 – 10 keV, 10 – 78 keV bands and the 10 – 78 keV / 3 – 10 keV hardness ratios. The observations, sorted and numbered by observation date (see Tab. 2), are color coded. The vertical dashed lines mark the positions where the x-axis is discontinuous because of long intervals between exposures.

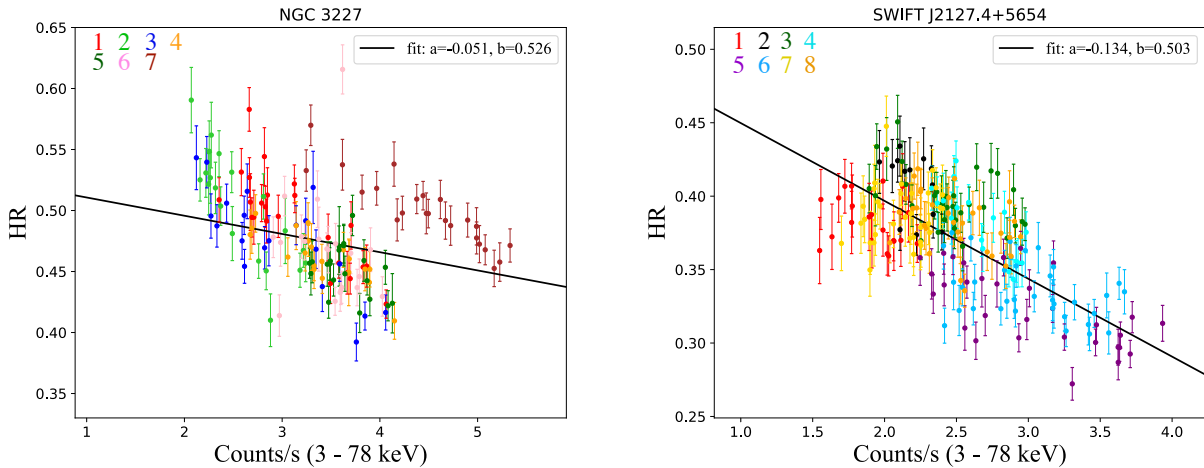


Figure 2. The 10 – 78 keV / 3 – 10 keV hardness ratio versus 3 – 78 keV count rate. The black lines show simple linear fits to the data points. The observations are color coded as in Fig. 1.

Table 1. NuSTAR Observation Logs.

Source	ID and No.	Obs. time	Exposure (ks)	Flux _{3–78keV} ($10^{-10} \text{erg/cm}^2/\text{s}$)
NGC 3227	60202002002 (1)	2016-11-09	49.8	1.26
	60202002004 (2)	2016-11-25	42.5	1.05
	60202002006 (3)	2016-11-29	39.7	1.16
	60202002008 (4)	2016-12-01	41.8	1.37
	60202002010 (5)	2016-12-05	40.9	1.38
	60202002012 (6)	2016-12-09	39.3	1.35
	60202002014 (7)	2017-01-21	47.6	1.8
	60402008002 (8)	2018-07-16	71.6	0.83
SWIFT J2127.4+5654	60001110002 (1)	2012-11-04	49.2	0.58
	60001110003 (2)	2012-11-05	28.8	0.71
	60001110005 (3)	2012-11-06	74.6	0.77
	60001110007 (4)	2012-11-08	42.1	0.82
	60402008004 (5)	2018-07-16	72.1	0.85
	60402008006 (6)	2018-07-30	72.9	0.66
	60402008008 (7)	2018-09-14	74.2	0.76
	60402008010 (8)	2018-12-30		

★: For convenience, the observations for each source were sorted and numbered (in parenthesis) by time.

volved. However, as further shown in §3, our study on the high-energy cutoff in this work is barely influenced by these complex absorbers.

Meanwhile, SWIFT J2127.4+5654, a radio-quiet NLS1 (Maliazzi et al. 2008) at $z = 0.0144$, has been observed by NuSTAR in two campaigns, with four exposures in 2012 and five in 2018. We dropped the observation 60402008002 (not listed in Tab. 1) of SWIFT J2127.4+5654, which has an issue flag = 1, indicating possible contamination from solar activity or other unexpected issues. Marinucci et al. (2014) performed a joint spectral fitting of the four 2012 observations with (quasi-)simultaneous XMM-Newton data and an average $E_{\text{cut}} = 108^{+11}_{-10}$ keV was reported. Besides, using XMM-Newton data only, Sanfrutos et al. (2013) reported a partial covering absorber in SWIFT J2127.4+5654 with $N_{\text{H}} = 2 \times 10^{22} \text{ cm}^{-2}$ and a covering fraction ~ 0.43 , whereas we find it has negligible effect in NuSTAR spectra.

NuSTAR data reduction is performed using the NuSTAR Data Analysis Software (NuSTARDAS) within the HEAsoft package (version 6.26). With CALDB version 20190513, the calibrated and cleaned event files are produced with *nupipeline*. We first extract the light curves using *nuproducts*, adopting a circular source region with a radius of $60''$ centered on each source, and an annulus from $120''$ to $200''$ for background extraction. The light curves from FPMA and FPMB, with the livetime, PSF/EXPOSURE and vignetting corrections applied, are then combined using *lcmath*. The $3 - 10$ keV and $10 - 78$ keV light curves, along with the $10 - 78$ keV/ $3 - 10$ keV hardness ratios, are plotted in Fig. 1. Both sources show clear variations in flux (count rate) and spectra shape (hardness ratio), not only between but also within the individual exposures. In the plot of hardness ratio (HR) versus count rate (Fig. 2) both sources clearly exhibit the “softer-when-brighter” pattern. However different individual exposures appear to follow different “softer-when-brighter” tracks. For instance, Obs. ID 60202002014 (No. 7) of NGC 3227 clearly deviate from other exposures in Fig. 2. See also exposures No. 1 and No. 2, No. 5 and No. 6 of SWIFT J2127.4+5654. Such variations could be due to the physical or structural changes in the corona which may lead to different “softer-when-brighter” tracks (e.g., Sarma et al. 2015), stopping us from merging data from different exposures according to the count rate or hardness ratio. In this work we focus on the analyses of spectra integrated over individual exposures and investigate the E_{cut} variations between these exposures. Though rapid hardness ratio variations within individual exposures are seen, due to limited photon counts we are yet unable to explore more rapid E_{cut} variations in two sources.

Source spectra are extracted from the same circular regions as the light curves, using the *nuproducts*. As for background extraction, we use NUSKYBGD developed by Wik et al. (2014) to handle the spatially variable background of NuSTAR observations (see also Kang et al. 2020, for an example). NuSTAR observations generally do not suffer from pile-up². Meanwhile, we find the low-energy effective area issue for FPMA (Madsen et al. 2020) to be insignificant in all the observations and no low energy excess in FPMA spectra is found (see Fig. A1). As a final step, the source spectra are rebinned to achieve a minimum of 50 counts bin⁻¹ using *grppha*.

We notice there are (quasi-)simultaneous XMM-Newton observations for both sources (six of NGC 3227 and three of SWIFT J2127.4+5654). However, we find slightly different photon indices between most XMM-Newton and NuSTAR exposures for both sources. Such discrepancy, likely due to the inter-instrument calibration, is widely found in literature (e.g. Cappi et al. 2016; Ponti et al. 2018; Middei et al. 2019b). Additionally, the fact that XMM-Newton and NuSTAR exposures are not perfectly simultaneous may also have played a role due to the intrinsic spectral variation. However requiring perfect simultaneity would yield significant loss of the valuable NuSTAR exposure time. Since E_{cut} measurement is sensitive to the photon index (e.g., Molina et al. 2019; Kang et al. 2020) and not all NuSTAR exposures have corresponding XMM-Newton observations, in this work we do not include those XMM-Newton exposures but provide uniform spectral fitting to NuSTAR spectra alone.

3 SPECTRAL FITTING

Zhang et al. (2018) developed the spectral ratio technique, analogous to the difference-imaging technique in astronomy, to assist the study of E_{cut} variations. Briefly, if the E_{cut} is invariable within two observations, the ratio of two spectra (primarily exponentially cutoff power law) is supposed to be a straight line in log-log space in the spectra ratio plot. So we can notice potential E_{cut} variations directly by looking for deviations from the straight line at the high energy end (see Zhang et al. 2018, for details). We applied this technique to AGNs with multiple archival NuSTAR exposures and took notice of NGC 3227 and SWIFT J2127.4+5654, of which the spectral ratios indicate clear and prominent E_{cut} variations as shown in Fig. 3. In this section, we perform spectral fitting to quantify the E_{cut} variations in both sources.

Spectral fitting is performed in the $3 - 78$ keV band within XSPEC (Arnaud 1996), using χ^2 statistics and the relative element abundances given by Anders & Grevesse (1989). All errors along with the upper/lower limits reported throughout the letter are calculated using $\Delta\chi^2 = 2.71$ criterion (90% confidence range). For each observation, the spectra obtained by the two NuSTAR modules (FPMA and FPMB) are fitted simultaneously, with a cross-normalization difference typically less than 5% (Madsen et al. 2015).

We employ *pexrav* (Magdziarz & Zdziarski 1995) to describe the exponentially cutoff power law plus the reflection component. For simplicity, the solar element abundance for the reflector and an inclination of $\cos i = 0.45$ are adopted (as default of this model)³.

² https://heasarc.gsfc.nasa.gov/docs/nustar/nustar_faq.html#pileup

³ These two parameters are poorly constrained with NuSTAR spectra if allowed free to vary, thus are commonly fixed at the default values in many studies on NuSTAR spectra (e.g. Zhang et al. 2018; Molina et al. 2019; Panagiotou & Walter 2020). Through joint fitting XMM-Newton and NuSTAR spectra of SWIFT J2127.4+5654, Marinucci et al. (2014) reported an iron

Table 2. Spectral Fitting Results.

ID and No.	N_{H} (10^{22} cm^{-2})	Γ	R	EW (eV)	E_{pexrav} (keV)	χ^2_{ν} (pexrav)	E_{pexriv} (keV)	χ^2_{ν} (pexriv)	E_{relxill}	χ^2_{ν} (relxill)	$kT_{\text{xillverCp}}$ (keV)	χ^2_{ν} (xillverCp)	$kT_{\text{relxillCp}}$ (keV)	χ^2_{ν} (relxillCp)
NGC 3227														
60202002002 (1)	$1.4^{+0.5}_{-0.5}$	$1.75^{+0.06}_{-0.06}$	$0.94^{+0.23}_{-0.2}$	100^{+16}_{-16}	185^{+115}_{-53}	1.05	248^{+254}_{-87}	1.05	128^{+43}_{-27}	1.09	24^{+5}_{-3}	1.1	24^{+5}_{-3}	1.11
60202002004 (2)	$0.5^{+0.8}_{-0.5}$	$1.63^{+0.09}_{-0.08}$	$0.73^{+0.26}_{-0.22}$	$211^{+49}_{-43} \star$	113^{+54}_{-28}	0.96	126^{+68}_{-34}	0.95	96^{+37}_{-17}	1.00	22^{+4}_{-4}	1.02	18^{+6}_{-1}	1.03
60202002006 (3)	$1.5^{+0.6}_{-0.6}$	$1.84^{+0.07}_{-0.07}$	$0.88^{+0.26}_{-0.22}$	97^{+18}_{-19}	> 247	1.16	> 280	1.15	236^{+300}_{-86}	1.15	> 35	1.17	> 74	1.19
60202002008 (4)	$1.1^{+0.4}_{-0.4}$	$1.88^{+0.05}_{-0.05}$	$0.88^{+0.22}_{-0.22}$	88^{+16}_{-16}	> 780	1.02	> 1000	1.03	> 350	1.04	> 43	1.03	> 65	1.06
60202002010 (5)	$0.8^{+0.5}_{-0.5}$	$1.88^{+0.06}_{-0.06}$	$1.04^{+0.26}_{-0.22}$	54^{+16}_{-16}	> 218	0.99	> 260	0.97	> 233	0.98	> 35	1.02	> 42	0.99
60202002012 (6)	$2.0^{+0.3}_{-0.5}$	$1.93^{+0.03}_{-0.03}$	$1.09^{+0.29}_{-0.24}$	74^{+17}_{-17}	> 247	0.93	> 680	0.92	> 210	0.94	> 31	1.00	> 33	0.95
60202002014 (7)	$4.1^{+0.4}_{-0.4}$	$1.9^{+0.05}_{-0.05}$	$1.21^{+0.22}_{-0.19}$	52^{+13}_{-13}	355^{+473}_{-133}	1.01	> 350	1.01	172^{+74}_{-39}	1.01	> 36	1.04	> 49	1.04
SWIFT J2127.4+5654														
60001110002 (1)	< 0.0	$1.88^{+0.05}_{-0.05}$	$1.54^{+0.43}_{-0.36}$	$135^{+39}_{-10} \star$	63^{+15}_{-10}	1.01	71^{+18}_{-10}	1.01	110^{+41}_{-13}	1.06	19^{+2}_{-2}	1.07	21^{+9}_{-2}	1.04
60001110003 (2)	$0.9^{+0.8}_{-0.8}$	$2.0^{+0.1}_{-0.1}$	$1.58^{+0.34}_{-0.43}$	41^{+33}_{-34}	109^{+90}_{-34}	0.96	135^{+46}_{-48}	0.97	181^{+113}_{-55}	0.98	35^{+26}_{-13}	1.03	38^{+33}_{-14}	0.98
60001110005 (3)	$1.3^{+0.4}_{-0.4}$	$2.04^{+0.06}_{-0.06}$	$1.95^{+0.35}_{-0.31}$	59^{+14}_{-14}	92^{+26}_{-17}	1.01	117^{+45}_{-26}	1.02	121^{+24}_{-23}	1.04	21^{+2}_{-2}	1.13	26^{+7}_{-5}	1.03
60001110007 (4)	$0.6^{+0.6}_{-0.6}$	$1.98^{+0.08}_{-0.08}$	$1.65^{+0.41}_{-0.35}$	44^{+17}_{-18}	67^{+18}_{-12}	0.96	76^{+25}_{-15}	0.96	108^{+32}_{-18}	1.02	18^{+1}_{-2}	1.03	21^{+7}_{-2}	1.00
60402008004 (5)	$0.9^{+0.4}_{-0.4}$	$2.17^{+0.06}_{-0.06}$	$1.83^{+0.33}_{-0.29}$	60^{+12}_{-12}	63^{+12}_{-9}	1.09	69^{+15}_{-10}	1.07	93^{+12}_{-12}	1.12	16^{+1}_{-1}	1.18	24^{+6}_{-4}	1.10
60402008006 (6)	$0.8^{+0.5}_{-0.5}$	$2.11^{+0.06}_{-0.06}$	$1.64^{+0.28}_{-0.28}$	$85^{+34}_{-22} \star$	72^{+17}_{-17}	0.93	85^{+23}_{-15}	0.94	100^{+23}_{-12}	0.96	18^{+1}_{-1}	1.03	28^{+9}_{-6}	0.95
60402008008 (7)	$0.4^{+0.6}_{-0.4}$	$1.98^{+0.08}_{-0.07}$	$1.81^{+0.41}_{-0.35}$	$115^{+41}_{-34} \star$	81^{+24}_{-15}	0.95	97^{+36}_{-21}	0.95	143^{+36}_{-26}	0.98	23^{+4}_{-3}	1.07	33^{+10}_{-8}	0.97
60402008010 (8)	$1.3^{+0.4}_{-0.4}$	$2.12^{+0.06}_{-0.06}$	$2.27^{+0.39}_{-0.34}$	58^{+14}_{-14}	90^{+25}_{-16}	1.03	113^{+42}_{-25}	1.05	123^{+26}_{-22}	1.09	18^{+1}_{-1}	1.19	28^{+8}_{-5}	1.07

*: In some observations a broad Fe K α line is statistically needed, with the corresponding EW marked with \star . NGC 3227: 60202002004, $\sigma=0.24^{+0.11}_{-0.10}$ keV. SWIFT J2127.4+5654: 60001110002, $\sigma=0.28^{+0.14}_{-0.12}$ keV; 60402008006, $\sigma=0.29^{+0.20}_{-0.15}$ keV; 60402008008, $\sigma=0.28^{+0.16}_{-0.13}$ keV.

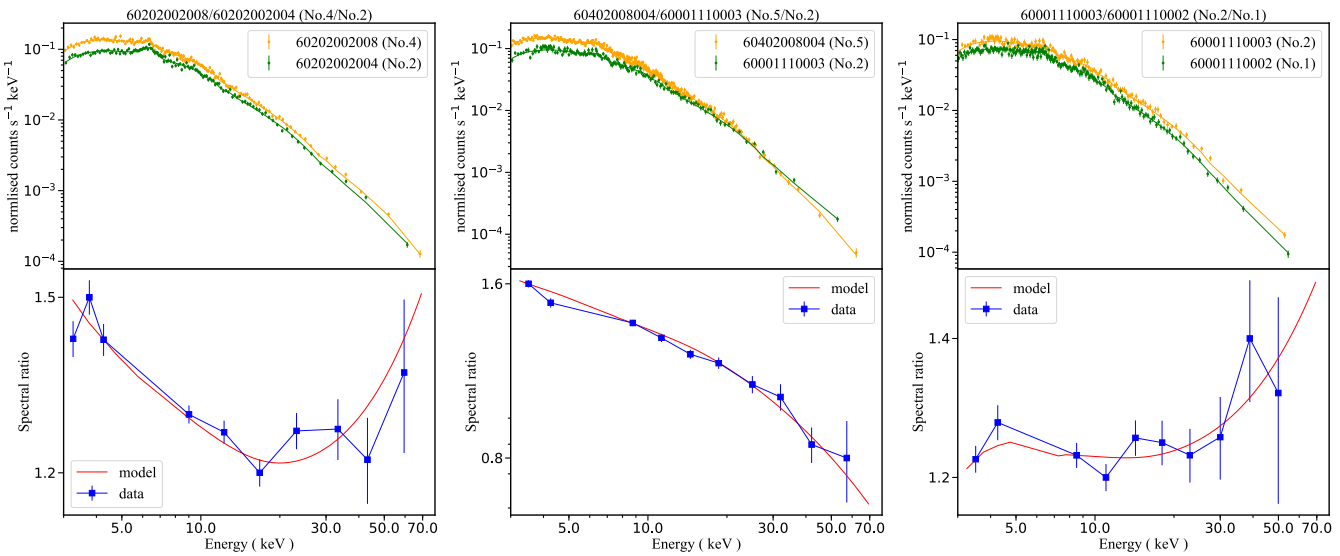


Figure 3. The rebinned FPMA spectra and spectral ratio (always the ratio of a brighter spectrum to a fainter one) of NGC 3227 (the left panel) and SWIFT J2127.4+5654 (the middle and right panels). Following Zhang et al. (2018), we adopt a single power law to fit each spectrum and derive the corresponding unfolded spectra for the calculation of spectra ratio. As approved in Zhang et al. (2018), the spectra ratio plot is insensitive to the adopted spectral model, except for in the spectral range of Fe K α line (which is dropped from the plot). For NGC 3227 we plot the ratio of the two observations showing the most prominent E_{cut} variation. The upward curvature in the lower left panel (deviation from a straight line at high energies) demonstrates clear ‘hotter-when-brighter’ pattern in NGC 3227. For SWIFT J2127.4+5654 we plot the ratios of two observation pairs, showing both ‘cooler-when-brighter’ (the downward high energy curvature in the lower middle panel) and ‘hotter-when-brighter’ (the lower right panel) patterns. In the lower panels, the ratios of best-fit models presented in this work are over-plotted, illustrating the E_{cut} variations have been properly accounted in the spectral models.

We let the photon index Γ , E_{cut} and the reflection fraction R free to vary. In addition, *zphabs* is used to model the intrinsic absorption,

abundance A_{Fe} of 0.71 and an inclination angle of 49°, slightly different from the default values we adopted. Generally, larger A_{Fe} (inclination angle) would yield slightly higher (higher) reflection fraction R , smaller (larger) photon index Γ and lower (higher) cutoff energy E_{cut} . However adopting different values of A_{Fe} or inclination angle would not alter the main results of this work.

with the Galactic absorption ignored due to its negligible impact on NuSTAR spectra. Replacing the *zphabs* component with *zxicpcf* to account for the partial covering reported in both sources (Turner et al. 2018; Sanfrutos et al. 2013) does not affect our E_{cut} measurements, as such absorbers have negligible influence on NuSTAR spectra.

As for the Fe K emission lines, several lines have been previously found in both sources with XMM-Newton spectra (e.g. Markowitz et al. 2009; Marinucci et al. 2014), whereas some of them are insignificant in NuSTAR spectra, likely due to the limited spectral resolution

(~ 0.4 keV at 6 keV). We use a statistical standard to model possible lines as follows. We add a *zgauss* component at 6.4 keV (rest frame) with its width fixed at 19 eV (the mean Fe K α line width in AGNs measured with Chandra HETG, Shu et al. 2010) to describe a neutral and narrow Fe K α line. Since the Fe K α line could be relativistically broadened, we allow the width to vary freely. If a free width can significantly improve the fit ($\Delta\chi^2 > 5$), the corresponding fitting results are adopted (see Tab. 2). Furthermore, we find no other potential lines in all the observations with this criterion. To sum up, our final model in XSPEC form is $\text{constant} \times \text{zphabs} \times (\text{pexrav} + \text{zgauss})$. The spectra and the best-fit models are shown in Fig. A1.

Besides, we adopt different models to check the results. Firstly we replace the *pexrav* component with *pexriv* (Magdziarz & Zdziarski 1995) to take account of potential ionized reflection. As shown in Tab. 2, the results of the two models (*pexrav* and *pexriv*) are very close. Furthermore, we employ *relxill* (Dauser et al. 2010; García et al. 2014) which models the spectra with a cutoff power law and relativistic ionized reflection from the accretion disc. For SWIFT J2127.4+5654 we fix its spin $a = 0.58$ referring to Marinucci et al. (2014), while for NGC 3227 a is tied among the observations during fitting, with $\log\xi$ and A_{Fe} tied among observations for both sources. In this way, we derive $a = -0.36^{+0.31}_{-0.22}$, $\log\xi = 2.65^{+0.07}_{-0.16}$ and $A_{\text{Fe}} = 2.78^{+0.61}_{-0.58}$ for NGC 3227, and $\log\xi = 2.80^{+0.05}_{-0.04}$, $A_{\text{Fe}} = 1.20^{+0.42}_{-0.25}$ for SWIFT J2127.4+5654. We let photon index Γ , reflection fraction and E_{cut} vary freely, and set other parameters including inclination and disk radii as default. As shown in Tab. 2, while the E_{cut} results from two models are generally consistent within statistical uncertainties, the *relxill* model yields systematically smaller E_{cut} for NGC 3227 and larger E_{cut} for SWIFT J2127.4+5654 compared with the *pexrav* model. Nevertheless, the yielded E_{cut} variation trends from two models, as the focus of this work, are similar. Moreover, we adopt comptonized models *xillverCp* and *relxillCp* (Dauser et al. 2010; García et al. 2014), for the normal and relativistic reflection components respectively) to directly measure the coronal temperature T_e . The derived coronal temperatures $kT_{\text{relxillCp}}$ and $kT_{\text{xillverCp}}$ (see Tab. 2) for SWIFT J2127.4+5654 are generally consistent with 1/3 of the measured E_{pexrav} (e.g. Petrucci et al. 2001), but systematically smaller than 1/3 of the best-fit E_{pexrav} for NGC 3227.

From Tab. 2 we can see that *pexrav* and *pexriv* yield similarly smaller reduced χ^2 compared with other models, while *pexriv* has one more free parameter than *pexrav*. As *pexrav* is widely adopted in literature to measure E_{cut} in literature (e.g. Zhang et al. 2018; Molina et al. 2019; Panagiotou & Walter 2020), to directly compare with those studies, hereafter we simply adopt the best-fit results from *pexrav*. Utilizing results from the other models however would not alter the conclusions of this work. Further note that in *relxill*, *relxillCp* and *xillverCp*, the reflection component and the Fe lines are coupled under certain assumptions, which may bias the E_{cut} (or T_e) measurements in some sources (e.g., Zhang et al. 2018; Kang et al. 2020).

We plot the E_{cut} vs. Γ contours in Fig. 4 to illustrate the E_{cut} variation patterns in two sources. A clear positive correlation between E_{cut} and Γ is seen in NGC 3227. However the E_{cut} - Γ plot of SWIFT J2127.4+5654 exhibits a distinct Λ shape: E_{cut} increases with Γ at $\Gamma \lesssim 2.05$, but reversely decreases at $\Gamma \gtrsim 2.05$. Though considering the degeneracy between E_{cut} and Γ , the rising part of the Λ shape is less significant comparing with the declining part, the overall variation trend in SWIFT J2127.4+5654 clearly deviates from a monotonous function. Meanwhile, the common “softer-when-brighter” trend in Seyfert galaxies is clear in both sources (Fig. 4).

To quantifying the significance of the Λ shape, we perform Spearman rank-order correlation analyses on the rising (obs. No. 1, 2, 3, 4, 7) and descending (obs. No. 2, 3, 5, 6, 8) branches of the Λ shape. We find a positive correlation between E_{cut} and Γ ($\rho = 0.87$ with a p-value = 0.054) for the rising branch, and a negative correlation for the descending branch (a $\rho = -0.90$ with a p-value = 0.037). We also perform linear regression to measure the slopes of the two branches of the Λ shape ($\beta = 220$ for the left and $\beta = -240$ for the right). However, the Spearman’s correlation could be unreliable when the sample size is small (e.g., $n < 10$), and random fluctuation can produce strong correlation/anti-correlation in small samples. Meanwhile, the measurement errors and the degeneracy of the parameters should also be taken into account. We perform simulations to address these issues. Assuming there is no intrinsic E_{cut} variation in SWIFT J2127.4+5654, we jointly fit all eight observations and derive a E_{cut} of 80 keV. Starting from $E_{\text{cut}} = 80$ keV and other best-fit spectral parameters (derived with E_{cut} tied) for each observation, we create one artificial spectrum for each exposure using *fakeit*. We then perform spectral fitting to those faked spectra to measure the simulated E_{cut} and Γ and perform Spearman rank and linear regression analyses. We repeat the process 1000 times, and find only 26 runs out of them show stronger Spearman’s correlation and steeper linear regression slope (compared with the observed values) for the left side of the Λ shape, while only 2 runs out of 1000 for the right one. This indicate the rising and descending of the Λ pattern have statistical confidence level of 97.4% and 99.8% respectively, showing statistical fluctuations of the parameters and the degeneracy between Γ and E_{cut} are unlikely able to reproduce the observed Λ pattern.

4 DISCUSSION

In Fig. 5 we plot $E_{\text{cut}} - \Gamma$ for both our sources together with those introduced in §1. For Ark 564 we convert the corona temperature kT_e given by Barua et al. (2020) into E_{cut} , assuming an optically thick corona and $kT_e \sim E_{\text{cut}}/3$ (Petrucci et al. 2001). For the other four sources we simply take measurements from Zhang et al. (2018). Though all of them follow the common “softer-when-brighter” trend (see Fig. 4 and Zhang et al. 2018; Barua et al. 2020), they show different $E_{\text{cut}} - \Gamma$ variation patterns. Interestingly, it appears that all seven sources could be unified with the Λ shaped pattern seen in SWIFT J2127.4+5654, e.g., “hotter-when-softer/brighter” at $\Gamma \lesssim 2.05$, but “cooler-when-softer/brighter” at $\Gamma \gtrsim 2.05$, though SWIFT J2127.4+5654 is the only source with Γ varying across the break point, thus the only one showing the complete Λ pattern in a single source.

The common “softer-when-brighter” trend in Seyfert galaxies was generally attributed to presumably cooler corona during brighter phases due to more effective cooling by more seed photons. However, such scenario clearly contradicts the discovery of “hotter-when-brighter” pattern detected in AGNs (e.g. Keek & Ballantyne 2016; Zhang et al. 2018). Geometry changes of the corona are required to reproduce the “softer-when-brighter” trend (e.g. Keek & Ballantyne 2016; Zhang et al. 2018; Wu et al. 2020). Specifically, the corona could be heated to a higher temperature and simultaneously driven to inflate during X-ray brighter phases (Wu et al. 2020), leading to a smaller opacity and thus softer spectra, and reproducing the observed “hotter-when-softer/brighter” pattern (the rising part of the Λ pattern). The inflation could be primarily vertical, as there are evidences that suggest the corona is vertically outflowing (e.g. Liu et al. 2014) and the corona could reach higher heights during brighter phases (Wilkins & Gallo 2015; Alston et al. 2020). Note in case of

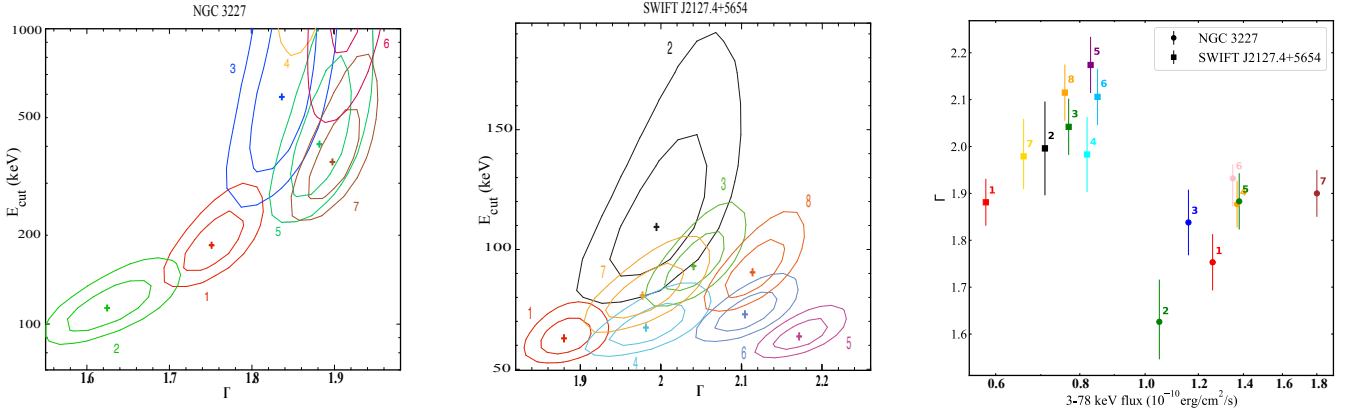


Figure 4. Contour plots (at 1σ and 90% confidence levels) of Γ vs. E_{cut} (Γ and E_{pexrav} from Tab. 2), and the Γ vs. 3–78 keV flux variabilities. The observations are sorted and numbered by observation date (see Tab. 2).

outflowing corona, if the outflowing velocity is higher during X-ray brighter phases, higher E_{cut} is also expected due to stronger Doppler shift.

As the X-ray flux brightening, spectrum softening and corona inflation continue, more seed photons from the disk could be intercepted, leading to higher cooling efficiency. Moreover, the cooling efficiency could be further boosted if the steeper X-ray spectrum is accompanied by a stronger soft X-ray excess component from the presumed warm corona (e.g. Petrucci et al. 2013) which could also contribute as seed photons. The latter mechanism may be essential, that the Compton cooling effect begins to dominate beyond a certain Γ , yielding the declining part of the Λ pattern (“cooler-when-brighter”). However, as SWIFT J2127.4+5654 is yet the only individual source showing a Λ pattern, it is unclear whether the break point of $\Gamma \sim 2.05$ is universal, and if yes, why so.

Meanwhile, pair production may also play a key role. As shown in Fabian et al. (2015), the coronae in many AGNs lie close to the electron–positron pair runaway line in the compactness–temperature diagram, suggesting the corona temperature is controlled by pair production. An inflated corona with a smaller compactness means a higher temperature limit by the run away pair-production. Moreover, Ghisellini & Haardt (1994) showed that, in a pair-dominated corona with a certain compactness, the temperature positively correlates with Γ for electron temperature $kT_e < m_ec^2$. Therefore positive correlations between X-ray flux and E_{cut} and between Γ and E_{cut} are expected in pair-dominated corona.

It is known that the NLS1 Ark 564 lies well below the thermal pair-production limit (Kara et al. 2017), meanwhile 3C 382, 4C 74.26, NGC 5548 and Mrk 335 lie close to the limit (e.g. Zhang et al. 2018). Following Fabian et al. (2015) we calculate the compactness, $l = 4\pi(m_p/m_e)(r_g/r)(L/L_{\text{edd}})$, and dimensionless temperature, $\Theta = kT_e/m_ec^2$, for the two sources reported in this work, where $kT_e \approx E_{\text{cut}}/2$ ⁴. We adopt $r = 10 r_g$ and the 0.1–200 keV luminosity, $M = 1.4 \times 10^7 M_\odot$ for NGC 3227 (Graham 2008), and $M = 1.5 \times 10^7 M_\odot$ for SWIFT J2127.4+5654 (Malizia et al. 2008). Comparing the results with the runaway pair production boundary in Stern et al. (1995), we find while NGC 3227 lies close to or on the boundary,

⁴ We adopt $kT_e \approx E_{\text{cut}}/2$ to stay consistent with Fabian et al. (2015) and Zhang et al. (2018). Directly adopting the $kT_{\text{relxillCp}}$ or $kT_{\text{xillverCp}}$ we derived, or assuming $kT_e \approx E_{\text{cut}}/3$ will not alter the main results presented here.

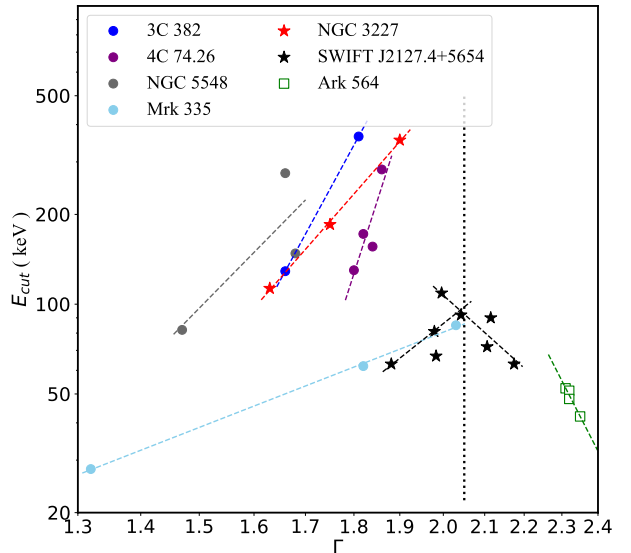


Figure 5. The $\Gamma - E_{\text{cut}}$ variation patterns of our two sources and those reported in literature. To avoid confusion, no error bars or contours are given, and we drop those exposures in which E_{cut} are non-detected. Besides, we dropped the data of 60002044006, NGC 5548, to avoid the potential photon index discrepancy issue, caused by XMM-Newton data as discussed in §2. A single best-fit direct line is over-plotted to demonstrate the overall variation trend of each source, except that for SWIFT J2127.4+5654 we plot two lines to illustrate the Λ shape. The vertical dotted line marks the transition to the left (right) of which E_{cut} positively (negatively) correlates with Γ .

the NLS1 SWIFT J2127.4+5654 also lie clearly below the boundary (though closer to the boundary compared with Ark 564, Fig. 6).

It is remarkable to note that there also likely exists a link between E_{cut} variation patterns and pair-dominance: pair-dominated coronae (those lying close to or on the pair limit in the $l-\Theta$ diagram) only exhibit “hotter-when-softer/brighter” trend, while a “cooler-when-softer/brighter” or Λ shape is only possible in coronae which are not pair-dominated. In this case the pair production could counter against the higher cooling efficiency of an expanded and less compact corona in many AGNs. Consequently the “cooler-when-softer/brighter” trend or the Λ pattern only exists in sources

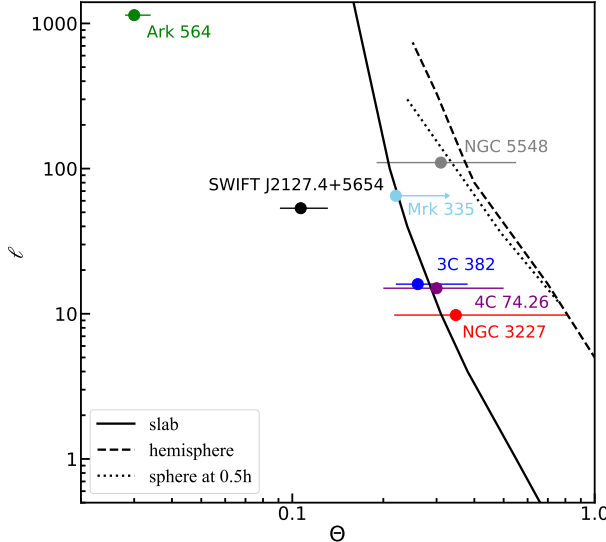


Figure 6. The l - Θ diagram of all seven sources. The results of Ark 564 in Kara et al. (2017) as well as the four sources in Zhang et al. (2018) are simply taken and plotted. The maximum temperature that can be reached by a plasma dominated by the runaway pair production for three geometries (Stern et al. 1995) are over-plotted as lines. For the four sources from Zhang et al. (2018) we take the data points from its Fig. 13 (the data point with the higher Θ for each source). For NGC 3227 and SWIFT J2127.4+5654 we plot the observation with the highest detected E_{cut} . For simplicity, no uncertainties to l are given.

lacking strong pair production, like the NLS1 SWIFT J2127.4+5654 and Ark 564. We note that Fabian et al. (2017) proposed that the coronae lying well below the pair limit (such as in Ark 564) could also be pair dominated if containing both thermal and non-thermal particles. However, if the possible link aforementioned does exist, it suggests the pair production in the cool coronae of Ark 564 and SWIFT J2127.4+5654 is indeed weak.

Though the sample discussed above is small, the discoveries presented in this work shed new light on the coronal physics in AGNs. Future observations of E_{cut} variations in a larger sample of AGNs are desired to testify the universality of the Λ pattern, confirm the potential link between E_{cut} variation pattern and pair production, and independently probe the coronal physics.

ACKNOWLEDGEMENTS

This research has made use of the NuSTAR Data Analysis Software (NuSTARDAS) jointly developed by the ASI Science Data Center (ASDC, Italy) and the California Institute of Technology (USA). The work is supported by National Natural Science Foundation of China (grants No. 11421303, 11890693 & 12033006) and CAS Frontier Science Key Research Program (QYZDJ-SSW-SLH006).

DATA AVAILABILITY

The data underlying this article are available in the article and in its online supplementary material.

REFERENCES

- Alston W. N., et al., 2020, *Nature Astronomy*, p. 2
- Anders E., Grevesse N., 1989, *Geochimica et Cosmochimica Acta*, 53, 197
- Arnaud K. A., 1996, in Jacoby G. H., Barnes J., eds, Astronomical Society of the Pacific Conference Series Vol. 101, Astronomical Data Analysis Software and Systems V. p. 17
- Ballantyne D. R., et al., 2014, *The Astrophysical Journal*, 794, 62
- Barua S., Jithesh V., Misra R., Dewangan G. C., Sarma R., Pathak A., 2020, *MNRAS*, 492, 3041
- Cappi M., et al., 2016, *A&A*, 592, A27
- Dauser T., Wilms J., Reynolds C. S., Brenneman L. W., 2010, *MNRAS*, 409, 1534
- Fabian A. C., Lohfink A., Kara E., Parker M. L., Vasudevan R., Reynolds C. S., 2015, *MNRAS*, 451, 4375
- Fabian A. C., Lohfink A., Belmont R., Malzac J., Coppi P., 2017, *MNRAS*, 467, 2566
- García J., et al., 2014, *ApJ*, 782, 76
- Ghisellini G., Haardt F., 1994, *ApJ*, 429, L53
- Graham A. W., 2008, *Publ. Astron. Soc. Australia*, 25, 167
- Haardt F., Maraschi L., 1991, *ApJ*, 380, L51
- Haardt F., Maraschi L., Ghisellini G., 1994, *ApJ*, 432, L95
- Harrison F. A., et al., 2013, *The Astrophysical Journal*, 770, 103
- Kang J., Wang J., Kang W., 2020, *The Astrophysical Journal*, 901, 111
- Kara E., García J. A., Lohfink A., Fabian A. C., Reynolds C. S., Tombesi F., Wilkins D. R., 2017, *MNRAS*, 468, 3489
- Keek L., Ballantyne D. R., 2016, *MNRAS*, 456, 2722
- Liu T., Wang J.-X., Yang H., Zhu F.-F., Zhou Y.-Y., 2014, *ApJ*, 783, 106
- Madsen K. K., et al., 2015, *ApJS*, 220, 8
- Madsen K. K., Grefenstette B. W., Pike S., Miyasaka H., Brightman M., Forster K., Harrison F. A., 2020, arXiv e-prints, p. arXiv:2005.00569
- Magdziarz P., Zdziarski A. A., 1995, *MNRAS*, 273, 837
- Malizia A., et al., 2008, *MNRAS*, 389, 1360
- Marinucci A., et al., 2014, *MNRAS*, 440, 2347
- Markowitz A., Edelson R., Vaughan S., 2003, *ApJ*, 598, 935
- Markowitz A., Reeves J. N., George I. M., Braito V., Smith R., Vaughan S., Arévalo P., Tombesi F., 2009, *ApJ*, 691, 922
- Matt G., et al., 2015, *MNRAS*, 447, 3029
- Middei R., et al., 2019a, *MNRAS*, 483, 4695
- Middei R., et al., 2019b, *MNRAS*, 483, 4695
- Molina M., Bassani L., Malizia A., Stephen J. B., Bird A. J., Bazzano A., Ubertini P., 2013, *MNRAS*, 433, 1687
- Molina M., Malizia A., Bassani L., Ursini F., Bazzano A., Ubertini P., 2019, *Monthly Notices of the Royal Astronomical Society*, 484, 2735
- Panagiotou C., Walter R., 2020, *A&A*, 640, A31
- Petrucci P. O., et al., 2001, *ApJ*, 556, 716
- Petrucci P. O., et al., 2013, *A&A*, 549, A73
- Ponti G., et al., 2018, *MNRAS*, 473, 2304
- Sanfrutos M., Miniutti G., Agís-González B., Fabian A. C., Miller J. M., Panessa F., Zoghbi A., 2013, *MNRAS*, 436, 1588
- Sarma R., Tripathi S., Misra R., Dewangan G., Pathak A., Sarma J. K., 2015, *MNRAS*, 448, 1541
- Shu X. W., Yaqoob T., Wang J. X., 2010, *The Astrophysical Journal Supplement Series*, 187, 581
- Sobolewska M. A., Papadakis I. E., 2009, *MNRAS*, 399, 1597
- Stern B. E., Poutanen J., Svensson R., Sikora M., Begelman M. C., 1995, *ApJ*, 449, L13
- Tortosa A., Bianchi S., Marinucci A., Matt G., Petrucci P. O., 2018, *A&A*, 614, A37
- Turner T. J., Reeves J. N., Braito V., Lobban A., Kraemer S., Miller L., 2018, *MNRAS*, 481, 2470
- Ursini F., et al., 2015, *A&A*, 577, A38
- Ursini F., et al., 2016, *MNRAS*, 463, 382
- Véron-Cetty M. P., Véron P., 2006, *A&A*, 455, 773
- Wik D. R., et al., 2014, *The Astrophysical Journal*, 792, 48
- Wilkins D. R., Gallo L. C., 2015, *MNRAS*, 449, 129
- Wu Y.-J., Wang J.-X., Cai Z.-Y., Kang J.-L., Liu T., Cai Z., 2020, arXiv e-prints, p. arXiv:2008.03284

- Zdziarski A. A., Poutanen J., Johnson W. N., 2000, [ApJ](#), **542**, 703
Zhang J.-X., Wang J.-X., Zhu F.-F., 2018, [ApJ](#), **863**, 71
Zoghbi A., et al., 2017, [ApJ](#), **836**, 2

APPENDIX A: NUSTAR SPECTRA

This paper has been typeset from a \TeX / \LaTeX file prepared by the author.

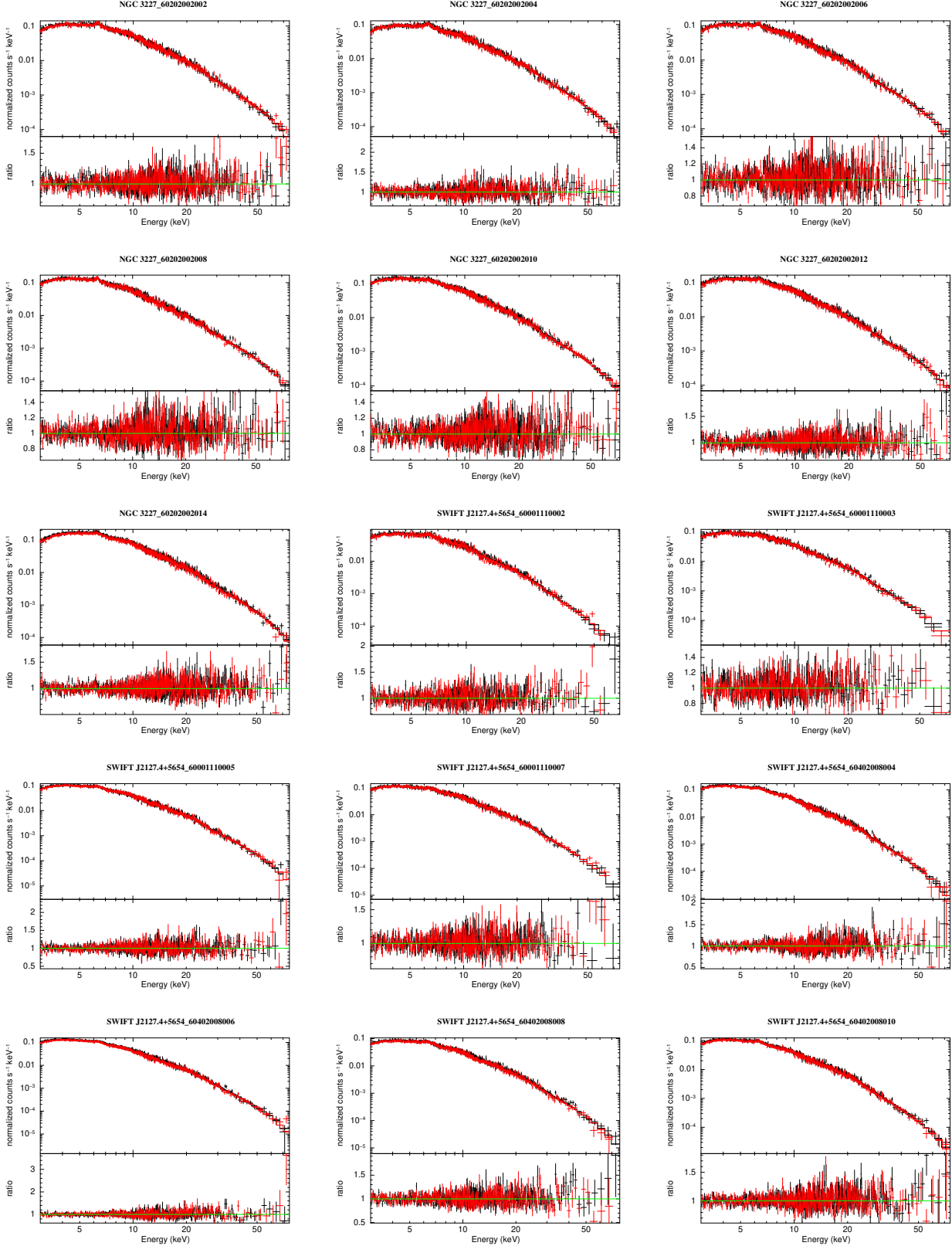


Figure A1. NuSTAR spectra, best-fit models (*pexrav*) and the residual data-to-model ratios. Spectra from both FPMA (black) and FPMB (red) modules are given. The best-fit spectral parameters are given in Tab. 2.